LAWRENCE
LIVERMORE
NATIONAL
LABORATORY

LLNL-JRNL-428612

Characterization of Escaping Electrons from Simulations of Hot Electron Transport for Intense Femtosecond Laser-Target Scenarios

L.Cottrill, M.Tabak, A.Kemp, R.J.P.Town

April 23, 2010

Nuclear Fusion

Disclaimer

Characterization of Escaping Electrons from Simulations of Hot Electron Transport for Intense Femtosecond Laser-Target Scenarios

L. A. Cottrill[1,2], A. Kemp[1], M. Tabak[1], R. P. J. Town[1]
[1]Lawrence Livermore National Laboratory
[2]Massachusetts Institute of Technology

Early experimental and analytical results for short pulse, high intensity laser-target scenarios have claimed the existence of significant surface currents along the target edge due to hot electron confinement by electromagnetic surface fields. However, more recent fully integrated explicit and hybrid-implicit PIC simulations have revealed that surface confinement is only a minor effect. This discrepancy can be attributed to an observational effect; only a small fraction of electrons escape and they may not represent the bulk distribution. PIC simulations reveal that enhanced surface emission is largely dependent on target geometry and has only a minor dependence on laser incidence angle and/or the angular distribution of the hot electron birth distribution. Furthermore, the escape distribution appears to differ from the initial birth distribution primarily at low energies and is higher in temperature, which is significant for the interpretation of experimental measurements.

I. Introduction

With the emergence of the fast ignition concept over a decade ago, relativistic electron generation and transport has gained an increasing level of attention [1]. The fast ignition scheme, an alternative to the conventional method of inertial confinement fusion, relies on a relativistic electron beam generated via a short-pulse, high intensity laser-plasma interaction to ignite a pre-compressed deuterium-tritium target. More recent schemes have embedded a guiding cone into the initial target to keep a corridor open that is relatively free of coronal plasma during the fuel implosion and also to minimize the beam propagation distance to avoid subsequent transport issues [2,3]. Early work claimed that the embedded cone also has the advantage that it can help to confine and guide electrons along its inner wall [4,5]. However, the degree of this confinement and guiding has been a subject of debate in recent years as a result of a number of inconsistencies that have arisen in experimental, analytical, and computational results. Given the importance of this issue for target design purposes and the interpretation of experimental measurements, the goal of this work was to investigate these inconsistencies by performing both integrated-explicit and hybrid-implicit PIC simulations of cone and slab geometries with laser parameters similar to early published results.

Sentoku,et.al., [20] in an early analysis of laser interactions cone showed energy concentration at the cone tip both by focusing the laser light to the tip and by transporting the hot electrons generated in interactions with cone wall to the tip. They showed that the electron energy density was concentrated in the very thin layers along the outer and inner surfaces of the cone. The calculations assumed a low density collisionless plasma(5 times critical density) and were of limited extent and duration(15 laser cycles). Later calculations by Nakamura,et.al.[18] over longer durations showed that the electrons penetrated the bulk of the plasma. These calculations had the cone illuminated all the way to the cone tip so that the electron production mechanism is closely tied to the electron transport mechanism. Experiments aimed at understanding the transport use finite spots and measure electrons outside of the laser field. One set of such experiments inject electrons into a wire or nail and track the electron flow down the wire[21,22]. Here the electrons were injected into the bulk of the plasma. Implicit PIC(particle-in-cell) calculations, describing those experiments using techniques similar to those used in this paper, claimed enhanced electron currents near the surface of the wire along with magnetic fields up to 50 MG(about 5% of laser field at at the end of the wire or nail. Another set of experiments looked for electron flows along surfaces by measuring the angular distribution of escaping electrons(Li et.al., Ping,et.al.). This paper will concentrate on understanding experiments of this sort.

The physical mechanism claimed by Nakamura et al. [4] for which hot electrons are confined to the target surface can be explained by the formation of electric and magnetic fields due to the interaction of an electron beam with a background plasma. Initially, electrons are generated during the laser plasma interaction due to collective absorption mechanisms such as Brunel heating, vacuum heating, etc. As the electrons are accelerated into the bulk target in the direction of the incident laser, they create a large magnetic field on the target surface, acting to reflect the remaining electrons that enter the target toward the vacuum region. In addition, a quasistatic electric field is also generated near the surface from the space charge that builds up as a result of electrons being pulled from the target by the laser electric field, acting to reflect electrons back into the bulk target. The counteracting nature of both the electric and magnetic fields results in a finite electron current flow along the cone surface that self-consistently enhances the initial fields. This mechanism leads to a “critical” cone angle below which no

further electrons would penetrate into the bulk target and all would simply be confined to the cone wall by the buildup of electromagnetic fields along the surface.

More recent experimental results by Li et al. involving oblique laser irradiation of planar foils using the Xtreme Light II laser system suggest that this surface confinement is less extreme [5]. Using a p-polarized pulse with an energy of up to 0.6 J in 30fs and a focal spot size of approximately 10μm, they measured angular distributions of fast electrons for different angles of laser incidence onto a 30μm thick aluminum target. Like Nakamura et al., their results show an increase in the number of electrons emitted parallel to the target surface as the laser incidence angle is reduced, with a maximum of around 50-65% for a 22.5º angle of incidence. This result was interpreted to indicate surface confinement, but their results did not show a "critical" angle below which 100% of the hot electrons were completely confined. In experiments using up to 20 J of P-polarized laser energy incident at 45^0 Ping, et.al. [11] saw the bulk of the escaping electrons emerge either along the laser direction(for J X B heating) or normal to the slab(for resonance absorption or Brunel heating). There were small jets along the target surface. Apparently, predominant flow of hot electrons along surfaces, which would be a boon for Fast Ignition, has not been universally observed.

As described in section II below we have been unable to reproduce these claimed dominant surface electron jets in PIC calculations. This failure occurred in both calculations where electrons were injected into the slab with a prescribed distribution (thereby testing the Nakamura model) and where the slab was driven by a laser. Electrons injected parallel to the surface did stay on the surface, however. We have been able to link these discrepancies to the idea of an observational effect where there are significant differences between the escaping hot electron distribution function and the original birth spectrum due to the generation of strong electrostatic self-fields [6]. In section III we show in a simple spherical model that the escaped electrons comprise only a small fraction of the hot electrons that were accelerated by the laser pulse and that even these electrons have their energies significantly modified. In section IV we describe 2D PIC calculations showing that angular distributions of the escaped electrons for several assumed electron birth distributions and slab dimensions. The electrons escaping along the surface outside the target that are measured are not representative of the hot electrons actually confined along the surface within the target. In other words, target geometry plays a

significant role in structure of the hot electron spectrum that is measured outside of the target. In section V we summarize the work.

II. Surface Transport

In an effort to investigate the actual hot electron surface confinement by electromagnetic fields, we utilized the hybrid-implicit PIC capabilities of the LSP code [7], as well as integrated explicit PIC simulations using the PSC code [8]. By utilizing both codes we were able to take advantage of a number of features unique to each in order to better understand the hot electron transport and cone-target physics. More specifically, PSC allowed for complete modeling of the laser-plasma interaction followed by subsequent hot electron transport down the target. Although this technique is very robust, it is also computationally expensive, given that explicit schemes must resolve both the plasma frequency and Debye length. However, the LSP code nicely complements this technique with its direct-implicit particle push and hybrid fluid-kinetic algorithm that allows for modeling of colder, denser plasmas for longer simulation times without having to resolve the plasma frequency and Debye length. Furthermore, the user also has complete control over the initial hot electron distribution, which allows him/her to understand basic transport physics using simpler problems without having to deal with the complications of the laser pulse and laser plasma interaction.

The simulation geometry, which is depicted in Fig. 1, was chosen to approximately mimic the analytical, experimental, and simulation targets in the publications of Li and Nakamura, claiming

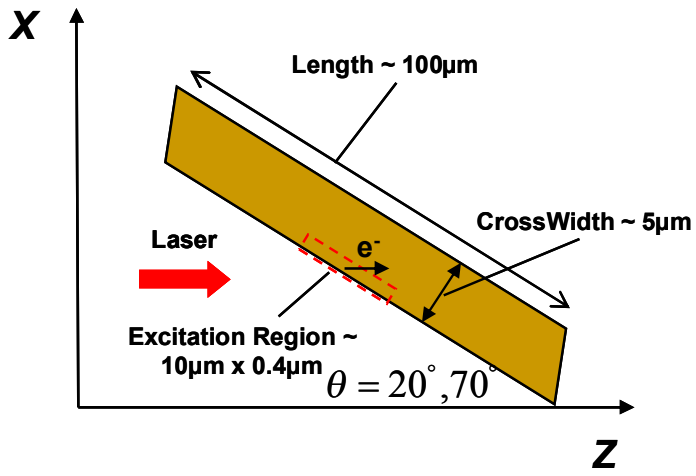

Fig. 1. LSP simulation geometry for modeling PIC and experimental laser-target problems of Li et al [5].

observation of surface electron currents . An aluminum slab, with the aluminum atoms triply ionized, 100μm long and 5μm thick was modeled in 2D Cartesian geometry to mimic the PIC/experimental geometry of Li et al [5]. Angles of 20° and 70° between the slab (or cone) surface and the electron beam drift direction were chosen to analyze the extent of increase in electron confinement as one moves to smaller target angles. LSP simulates laser conditions by promoting hot electrons from a cold fluid electron background. Electrons were excited with a Jüttner momentum distribution, with temperature and drift parameters of 305 keV and 0.5c, respectively, which are approximately consistent with parameters fit from data obtained by Li et al. A total of 0.30 Joules of energy were injected into the problem over a 30 fs Gaussian pulse in the form of hot electrons by promoting from a region along the upper cone, which was 10μm long and 0.4μm thick.

Before directly comparing confined electron fractions, we first compare the magnitudes of the surface electric and magnetic fields with published PIC results by Li et al. They used an explicit PIC code that included modeling the laser-plasma interaction. From

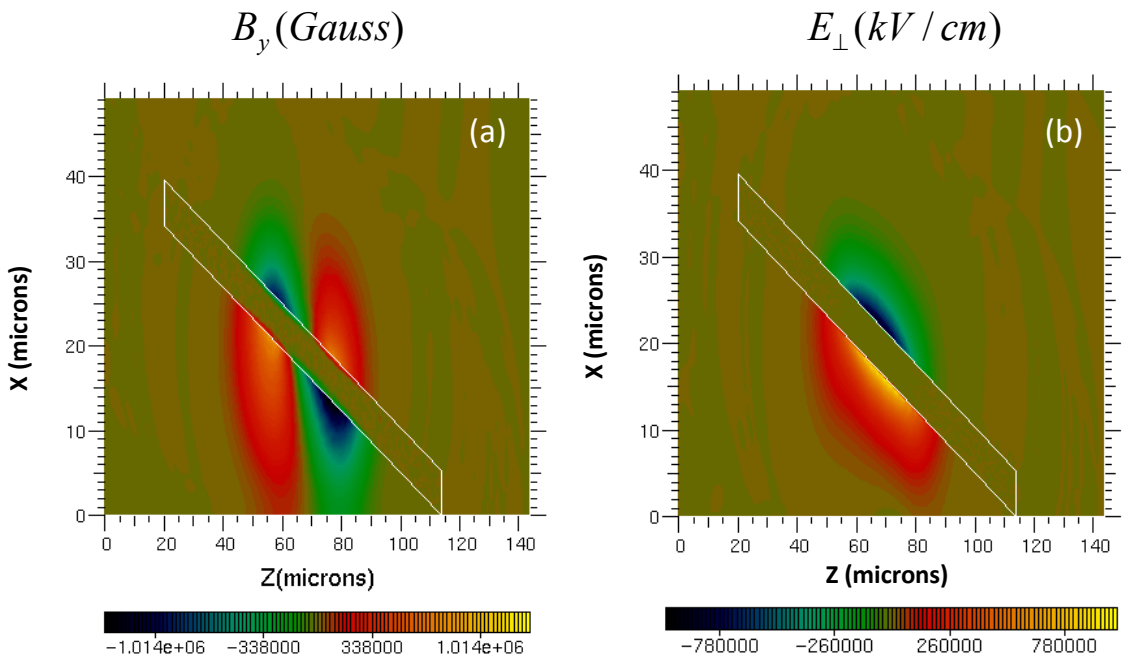

Fig. 2. Surface (a) magnetic and (b) electric fields produced from LSP simulation.

their simulations, they quote a peak surface magnetic field of approximately $2x10^7$ Gauss and a peak surface electric field of approximately $6x10^6$ kV/cm. These values agreed with our PSC [8] results (B_{peak} = 1-$2x10^7$Gauss; E_{peak} = 3-$5x10^6$ kV/cm), they differ substantially from those of LSP. As one can see in Fig. 2, the surface magnetic and electric fields peak at approximately $1.4x10^6$ Gauss and $1x10^6$ kV/cm, respectively, which are 6-15 times lower than the values obtained by the calculation of Li et al. that included the laser-plasma interaction [5]. The laser-plasma interaction can locally generate quasistatic fields larger than those generated by the hot electron current alone.

The large difference between the magnetic fields measured in our simulations when a spot is driven by a laser and when the energy is delivered into the plasma as a distribution of very energetic electrons illustrates the important role that the oscillating laser field has in setting up a quasistatic field. The quasistatic magnetic fields thus produced have magnitudes comparable to the laser field. These large fields have been seen in simulations[12,13] and measured in the laboratory [14,15]. Sudan [16] followed by Mason [13] pointed out the importance of the ponderomotive force acting on the background electrons and separating the forward current from

the return current provided by the background electrons. In the earliest use of the implicit-PIC method[23] for electron=plasma transport problems, Brackbill and Forslund accounted for the effect of resonance absorption by accelerating electrons out of the plasma with density twice critical density into the vacuum and toward the laser. This uncompensated current produced magnetic fields comparable to those of the laser driving the experiment. These fields drove the electrons across the surface of the slab and led to a large fraction(30%) of the laser energy driving a fast ion blowoff.

In the case where we just inject electrons into a plasma that is not affected by the ponderomotive force, this current separation does not occur and the forward current is partially neutralized by the background plasma. A significantly lower magnetic field results. This is the situation in some experiments where an intense, small laser spot illuminates a slab and the hot electrons are measured some distance from where they are produced.

A complete treatment of current propagation in the presence of the laser field requires treatment of the oscillatory dynamics. For instance, Lasinski,et.al.[17] show weak current generation along the side of a cone. The electrons composing this current were drawn out from the overdense plasma into the vacuum and then accelerated by the laser wave. These electrons were arranged as series of bunches parallel to the cone surface. The self-consistent model described by Nakamura,et.al. [4] , where an external oscillatory field is not explicitly mentioned is more naturally used to describe the steady currents and fields produced when an electron beam is injected into a plasma.

The angular distribution of the electrons produced in this laser spot can be modified by the quasistatic fields in the spot. This paper will be concerned with the transport of electrons outside of the laser spot.

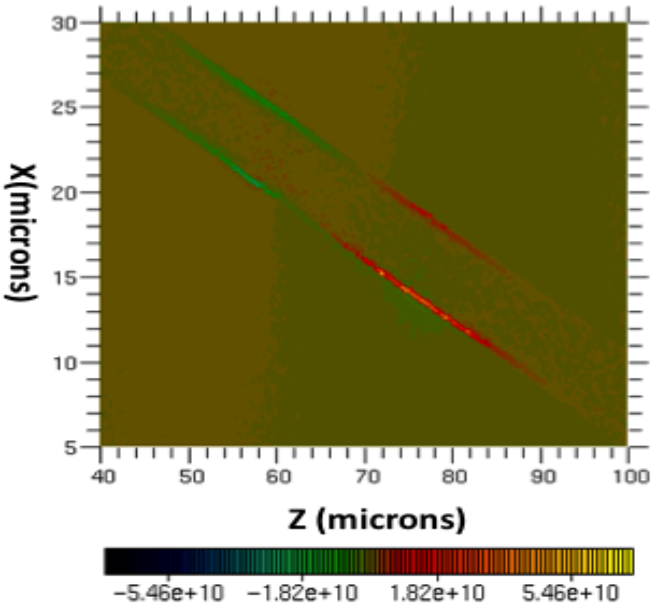

Figure 3. Component of current density aligned with slab

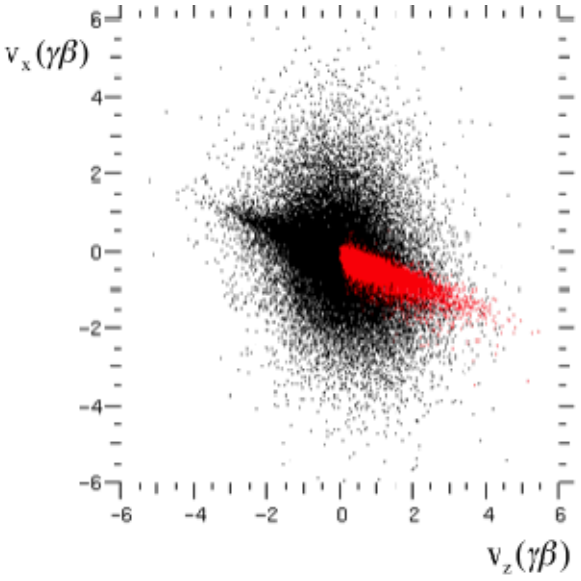

Figure 4. Momentum space distribution of hot electrons within -.4/.6 microns of surface. Red(electrons moving down surface);black(all hot electrons)

Figure 3 shows the component of the total current density aligned with the slab. This current density is concentrated near the slab edges. Figure 4 shows the momentum space distribution of the hot electrons taken from the region where there is a large current density (-.4/+.6 microns from the slab surface). The black points are all selected hot electrons, while the red points represent those that move down the surface. The particles moving down the surface are those that remain in this volume over 10 simulation time steps. Shown in Table 2 are, as functions of the angle between the beam centroid and the tangent to the surface, the fraction of the total hot electron population within -.4/+.6 microns of the surface that is moving down the surface, the

fraction of the electrons in the surface volume moving down the slab and the fraction of the total hot electron energy moving along the slab surface.

	20º	**70º**
n_{surf}/n_{total}	1.%	0.1%
$n_{surf}/n_{surftotal}$	33%	12%
E_{surf}/E_{total}	5%	0.03%

Table 2. See text for description

Shown in Table 3 is a compilation of surface and energy fractions computed for three different simulations using the experimental conditions described by Li et. al. [5] that were run with variations in geometry and with collisions turned on/off. As one can see from the data, the 0.4-0.7% surface confinement for the aluminum slab case, is substantially lower than the 50-65% confinement quoted in Li et.al.[5]. Although the inclusion of collisions in the simulation did result in a slight enhancement in both electron confinement and energy carried along the surface, the increase was not enough to produce agreement with the fractions of Li et al. This enhancement can be understood if one considers that scattering will have minimal effect on the higher energy electrons, allowing those particles to continue to travel along an approximately linear path determined by the angle at which they are born. However, moderate to low energy particles that may have not been born with energies and angular orientations that make them

Simulation	Fraction of hot electrons traveling down the surface	Fraction of energy carried down the surface
Al slab (no collisions)	0.5%	9%
Al slab (collisions)	0.7%	12%
Al cone (no collisions)	0.4%	8%

Table 3. Fraction of hot electrons traveling along the surface and fraction of energy carried along the surface for three simulation cases using various geometries and with collisions turned on/off.

vulnerable to confinement may be scattered into the surface region where the electromagnetic fields are strongest, resulting in an enhancement of confined electrons due to collisions.

We also examined the effect of geometry on surface confinement. More specifically, does a cone geometry, which is the target geometry currently being explored for fast ignition, result in more or less hot electrons being confined to the surface? As one can see from Table 3, both the surface confinement fraction and fraction of energy carried along the surface for the cone geometry are slightly reduced from that of the infinite slab. We note, however, that the cone in Fast Ignition experiments is illuminated by the laser for its entire extent so the conclusions of this LSP study, where the wall is not subject to the ponderomotive force, may not extend to the Fast Ignition cone. On the other hand, our limited set of PSC calculations(with incident laser), as well as Nakamura07[18] show that the hot electrons are not confined to a thin surface layer.

We modeled the complete interaction of the laser with the plasma slab in PSC calculations. A laser with peak vacuum intensity 1.4 10^{19}W/cm^2 was incident on a slab of plasma 5 microns thick and 300 microns long at density 30 times critical density at 75^o from the slab normal. The laser spot had FWHM 10 microns. The pulse has FWHM 120 femtoseconds. This case showed some transport along the slab. When the incident angle was 45^o no distinct surface current was observed. Figure 5 shows the energy density of all electrons with energy above 1 keV in the slab at two different times. The electron energy density is approximately uniform across the slab. There is a slight excess along the slab surface. At late times we see that the bulk of the energy density remains where the laser was incident. At the head of the electron pulse, the energy density is concentrated near the slab surface with some escaping the slab altogether. We identify this excess energy density with the electrons having kinetic energy greater than 1 MeV. Figure 6 shows how finite pulses of these energetic electrons propagate along the target. Associated with these pulses are self-consistent electric and magnetic fields as discussed in reference 4. The cycle-averaged magnetic field is about 10% of the vacuum laser field hundreds of femtoseconds after the laser has been turned off. Figure 7 shows the momentum distribution of the electrons at 1000 femtoseconds. The energetic electrons remaining in the simulation are mainly aligned with the slab surface or with the laser specular direction. The energetic electrons produced by the laser, but not aligned in these directions have escaped from the problem or given up their energy to the background plasma by driving a foil expansion. Figure 8 shows the total energy in these energetic electrons within 5 microns of slab

center and facing the laser side of the slab as a function of time. Most of these electrons are in a sub-micron region just outside the slab. For a total laser energy of 1600J/cm only 300 J/cm is coupled to electrons in the target. Of the total coupled energy at peak of 65J/cm appears as >1MeV electrons traveling along the surface. At the end of 200 microns travel down the slab, only 5.5J/cm remains;2% of the coupled energy and 0.4% of the incident laser light. We checked this result by extending the duration of the laser pulse to 1 ps. In that case 4% of the coupled electron energy remained as fast electrons propagating down the surface, with much of that near the laser spot. These surface confined electrons will be of small importance in transporting energy to the fusion region in Fast Ignition applications.

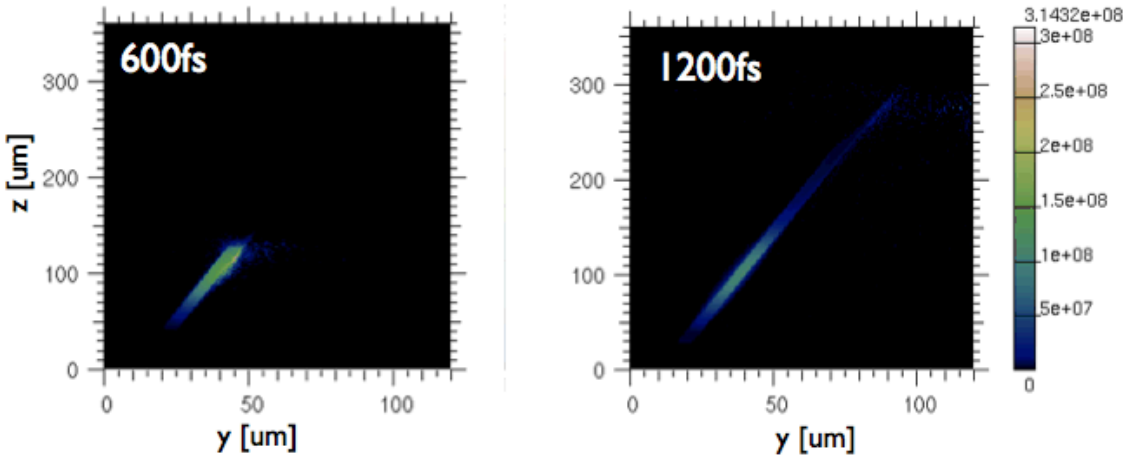

Figure 5. Energy density of all electrons with energy greater than 1 keV at 2 times. At 600 fs the energy within an area bounded by the slab center line and a line with axial coordinate 5 microns greater than the center line is 290 J/cm ;at 1200 fs 218 J/cm .

In order to understand how electrons are confined to the surface we tracked tracer particles as they reacted to the fields produced in the simulation in a slab geometry in our LSP calculations . The tracer particles were generated with energies ranging from 500 eV to 1 MeV and their directions relative to the z-axis varied from 0^o to -50^o . The slab has an angle of -20^o with the z-axis. In figure 9 we show the trajectories for -20^o and -50^o. For -20^o the particles are aligned with the surface and stay on the surface, while for other angles the particles quickly leave

the surface. If the laser-plasma interaction produces particles moving along the surface, they will stay on the surface. Particles traveling into a slab embedded in vacuum may be electrostatically

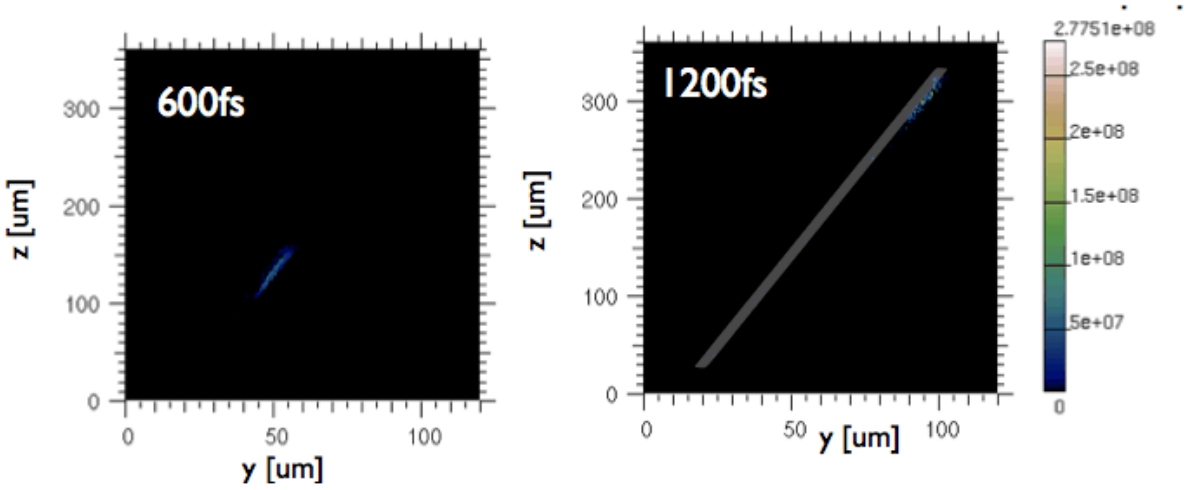

Figure 6. Energy density of all electrons with energy greater than 1 MeV at 2 times. At 1200 fs the original plasma slab has been added and the density has been multiplied by 10 to enhance the picture contrast.

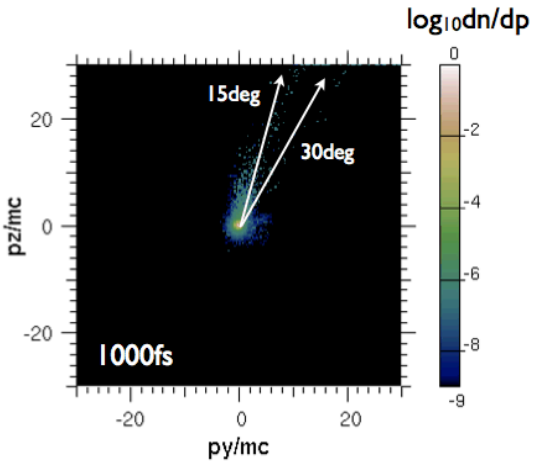

Figure 7. Electron phase space at 1 ps

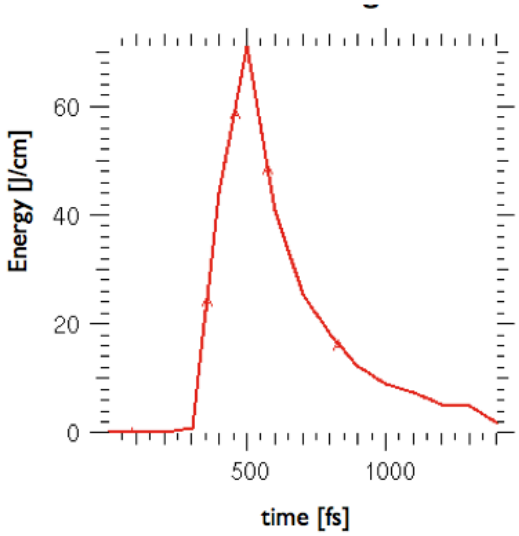

Figure 8. Energy in electrons with kinetic energy > 1MeV within an area bounded by the slab center line and a line with axial coordinate 5 microns greater than the center line.

confined by the slab and will diffuse within the slab until they lose their energy or find the end of the slab or cone. However, for Fast Ignition applications, the cone will be embedded in a plasma resulting from a capsule implosion and electrostatic confinement will not be available.

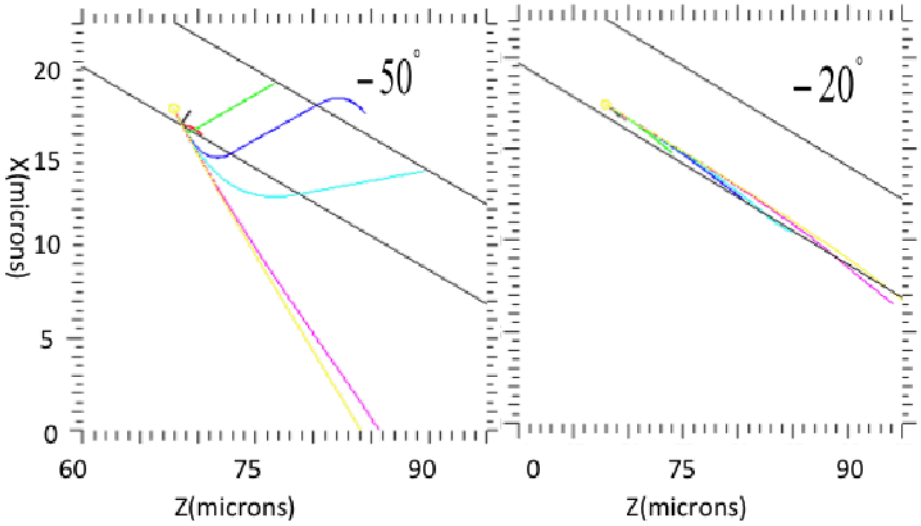

Figure 9. Trajectories of marker particles in slab geometry.

II. Simplified treatment of escaping electrons

Our simulations of electrons propagating in slabs did not reproduce the large fraction moving parallel to the slab surface that was observed in Li's experiment. However, Li et.al. did not measure the electrons in the slab. They measured electrons that had escaped. Could the escaping electron distribution function be very different from the distribution on the slab? In this section we show that self-consistent fields trap electrons near the slab and that the fraction of escaping electrons depends strongly on the scale of the emitting surface.

We use a simplified version of Fill's model [6] to estimate the fraction of source electrons that escape from the surface of a sphere. We calculate the escaping electron distribution function from a putative birth distribution as a function of sphere radius, source duration and injected energy. In our model we assume electrons escape to infinity with their birth energy less the energy lost travelling from the sphere center and surface and the potential energy difference between the sphere and infinity. The potential is determined by the previously escaped charge. We neglect the possibility that particles will pass each other in radius during the escape. Therefore, the potential affecting a particle is unchanged after it is launched. A more realistic treatment of crossing particles will be given in the next section.

The energy coupling efficiency from laser light to electrons,η, and the electron birth distributions are still areas of active research. We use a simple fit to Yasuike's [9] electron coupling measurements:

$\eta = \max[1.2\log_{10}(I/10^{18}\mathrm{W/cm^2})]$, where I is the incident intensity. We assume an electron energy distribution function based on recent simulations by B. Chrisman, et.al. [10], where part of the distribution is given by the ponderomotive scaling and a smaller fraction is has a temperature a quarter of the ponderomotive temperature. The electron distribution functions are known to be functions of preplasma conditions as well as peak plasma density and scaleheight. Our choice here will not be universally correct but it illustrate how escaping electron distributions can differ from the birth distributions. The instantaneous electron number birth distributions are then given by $f(E) \propto 0.5\exp(-E/t1)/\overline{E_1} + 0.3\exp(-E/t2)/\overline{E_2}$, where E is the electron kinetic energy, t1 (MeV)=$(I/10^{19}\mathrm{W/cm^2})^{1/2}$ and t2=0.25*t1. The incident laser power is given by $P(W/cm^2) = P_{\max}\cdot\exp(-t^2/2\sigma^2)$ σ is the half-width-half-maximum (HWHM) divided by $(2\log 2)^{1/2}$. We drive the plasma for +/-14 ½ σ. We assume the light is incident on an area of 3.5 $10^{-7}\mathrm{cm^2}$. The emitting surface is a sphere of radius R.

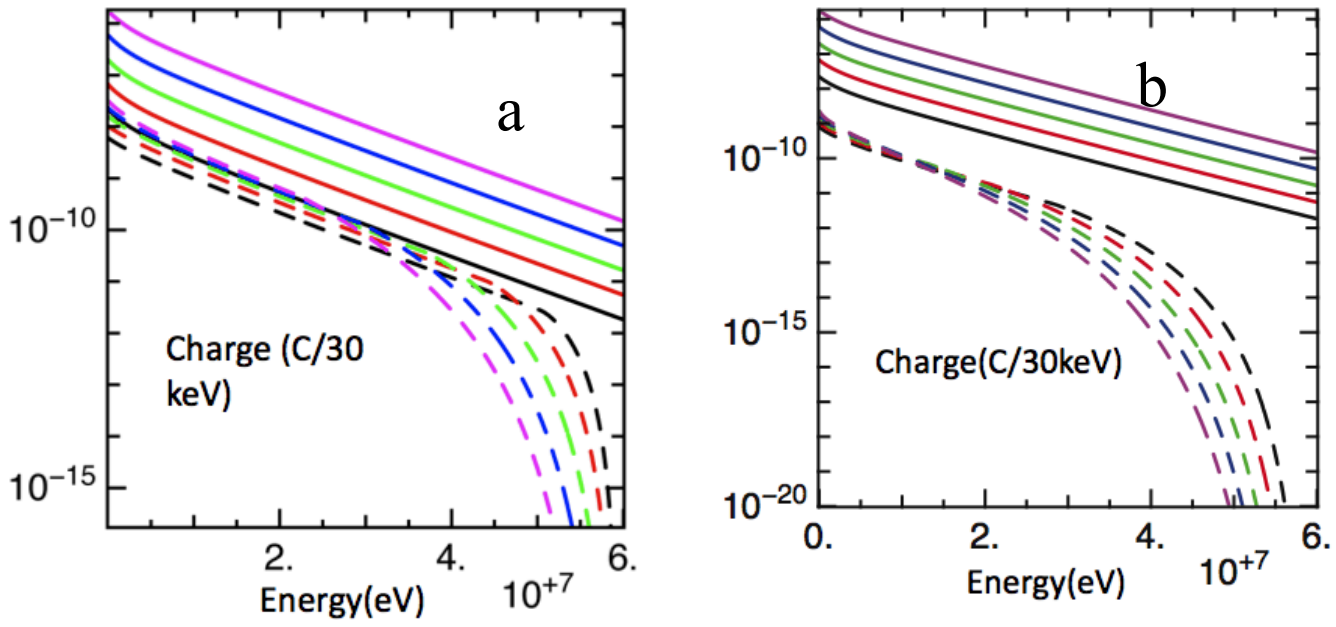

Figure(10). Source electron distributions (solid lines) and escaped electron distributions (dashed lines) for R=1mm (a) or R=30 micron (b) for P_{max}=200TW and HWHM = 50fs [1/81,1/27,1/9,1/3,1] for [black,red,green,blue,magenta]

We can now study how the emitted electron spectra change was we change the laser power (and intensity), the duration of the irradiation and the size of the emitting sphere. In Figure 10 we vary the laser duration for 2 values of emitting radius and fixed peak power. We see that escaped electron temperatures are similar to the source temperatures for the larger emitting radius. There is significant softening of the spectrum for the longer duration illuminations when emitted from a 30 micron radius surface. We would expect larger discrepancies in spectral shape if the source functions had sharp features at low electron energy. The charges are trapped much more in the small-radius emitting surface than in the larger radius. These behaviors are also exhibited in Figure 11 where we vary the peak power for fixed pulse length. Figure 8 shows increased escape inhibition and spectral softening as we reduce the emission radius for fixed peak power and duration. Based on these results one might expect that electrostatic inhibition would play a role in modifying angular distribution of electrons escaping from aspherical objects like slabs or disks.

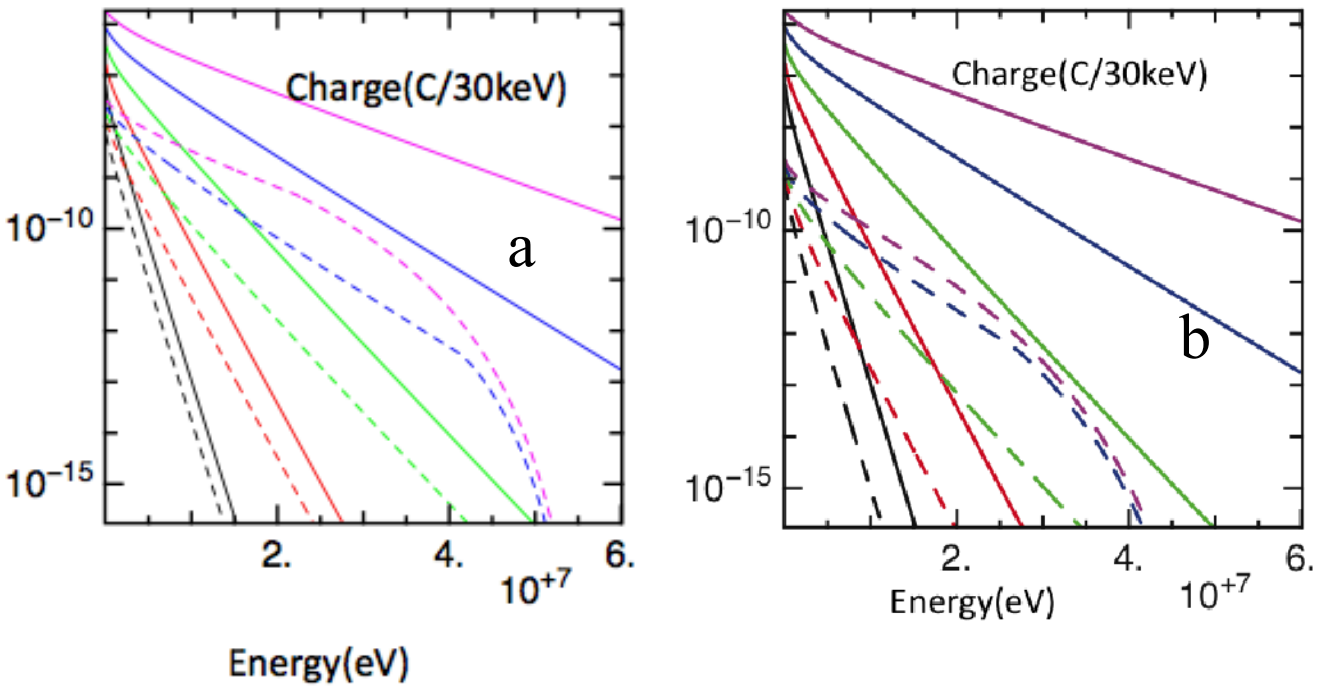

Figure(11)Source electron distributions(solid lines) and escaped electron distributions(dashed lines) for R=1mm(a) and R=30 microns(b),HWHM=50fs,Pmax(TW)=[2.4,7,22,67,1] for [black,red,green,blue,magenta]

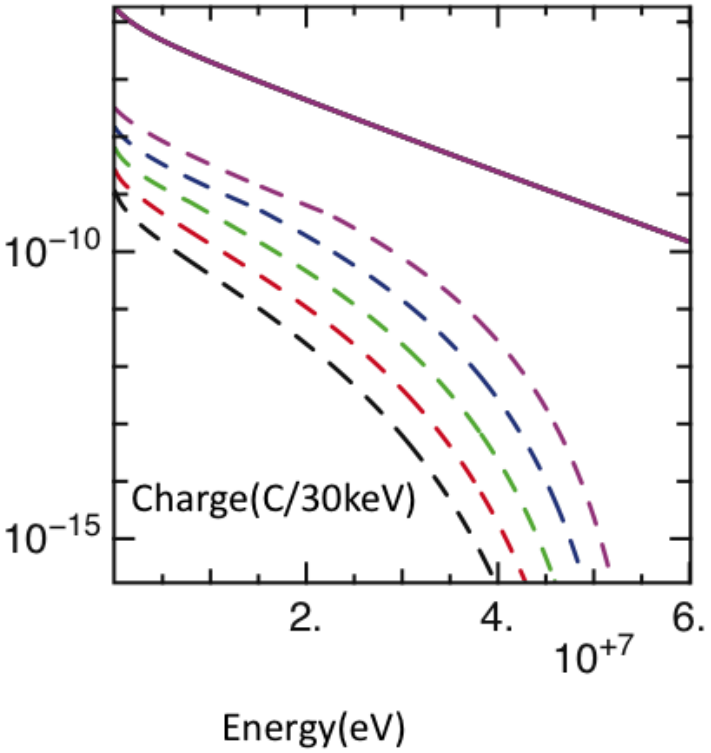

Figure(12).Source electron distributions (solid lines) and escaped electron distributions(dashed lines) for HWHM=50fs,Pmax=200TW,R=[1/81mm,1/27mm,1/9mm,1/3mm,1mm] for [black,red,green,blue,magenta]

Escape distributions from slabs

We used LSP to calculate the angular distribution of electrons escaping from slab targets. The targets that were modeled in these simulations were representative of the experimental targets of Li et al. mentioned previously [5]. Because the 2-D Cartesian geometry used in previous simulations doesn't capture the correct radial fall-off of the fields, cylindrical *R-Z* geometry was used for these simulations. The target geometry consists of a 100µm radius x 30µm thick collisionless aluminum disk bounded by vacuum in a region with 500µm radius and 500 µm axial extent. Hot electrons were promoted from a region of radius 10 µm and thickness 1 µm on the left surface of the disk over a Gaussian temporal pulse of 30fs with a total energy of 0.30 J, which corresponds to approximately 50% of the total energy of the laser pulse quoted by

Li et al [7]. The structure of the hot electron distribution involved use of an isotropic Jüttner (relativistic Maxwellian) with a 305 keV temperature, which is approximately consistent with parameters fit from data obtained by Li et al.

Shown in Fig.13 is the hot electron density and corresponding electrostatic potential at t = 600fs, which is well after the end of the source electron duration. As one can see, the hot electrons are initially emitted isotropically from the excitation region in a front or "shell-like" fashion. However, once the first wave of electrons leave, the target then acquires a positive charge, resulting in the buildup of large electrostatic fields and a subsequent sheath around the target edges. This redistribution of charge over time can be seen in the plot of electrostatic potential shown in Fig.13(b), revealing an increasingly large potential drop that develops across the target. The consequence of these electrostatic fields is that higher energy electrons with sufficient energy to overcome the sheath will escape from the target while the lower energy electrons will simply

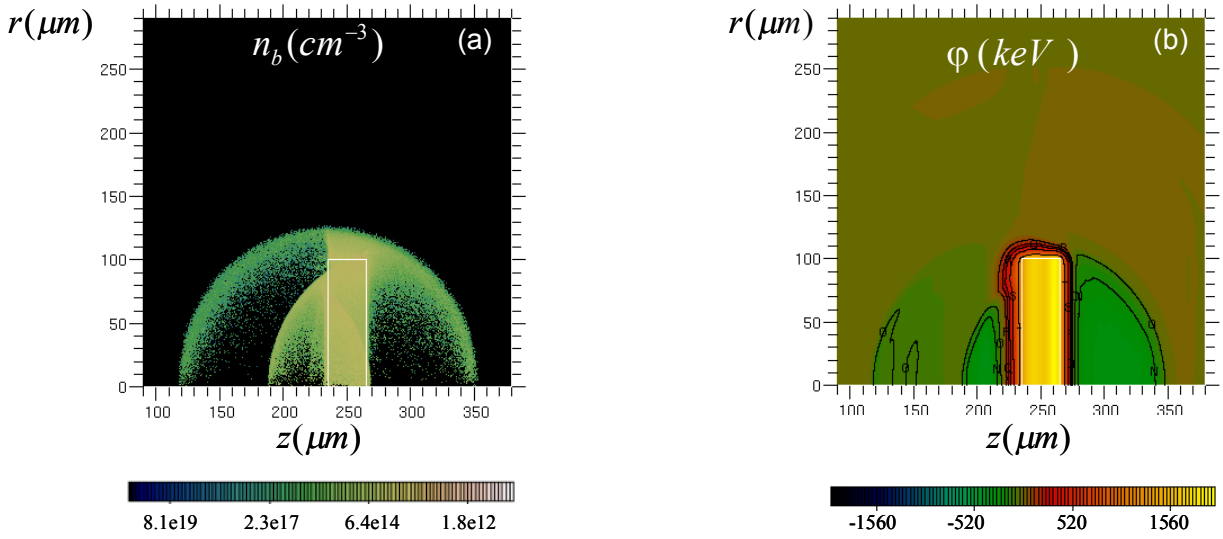

Figure 13.Hot electron density (a) and electrostatic potential (b) for a 2D LSP simulation of an isotropic hot electron source of 0.3J over a 30 fs Gaussian pulse.

reflux, or bounce, back towards the front edge with a redirected transverse momentum. Eventually, those electrons that continue to reflux within the target reach the top edge, at which point they then have a higher probability of escaping due to the lower potential drop at the top of the target compared to the potential drop across the sides, as shown in Figure13b. This effect can also be seen in the angular distribution shown in Figure 14(a) by the dominating peak around

90°, which corresponds to a large escape emission from the top edge of the target. The lesser peak near 135° is produced by electrons that bounce off the back surface and find a low potential region on the front surface from which to escape. In sum, by

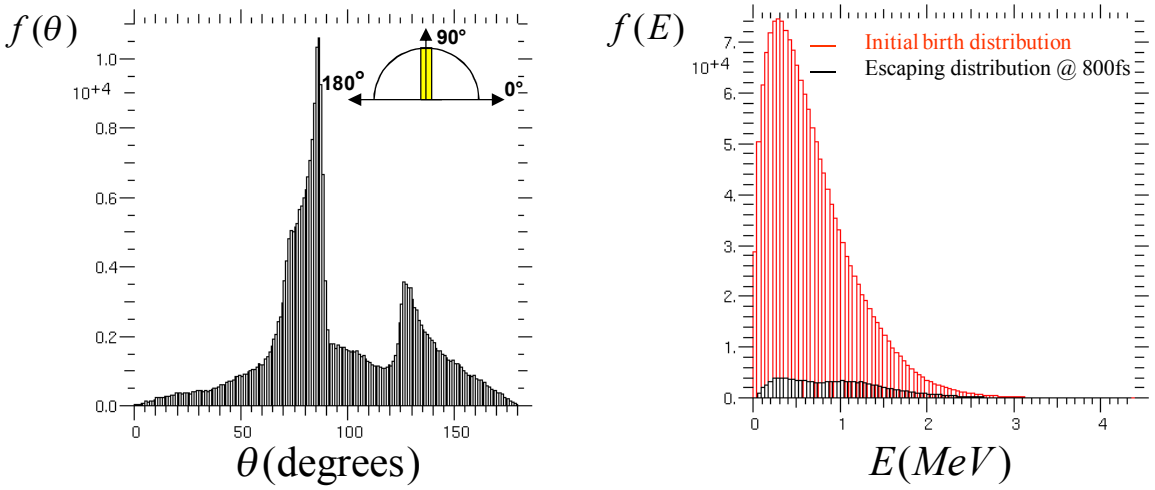

Fig. 14. Angular distribution of escaping electrons (a) and a comparison of the energy spectrum of the initial birth distribution and escaping distribution (b).

characterizing the escaping distribution, rather than the distribution along the actual surface, we were able to achieve better agreement (~31%) with the experimental measurements of surface escape electrons (28-50%). From this we were able to conclude that surface confinement is only a minor effect and the large surface fractions are an artifact of the target geometry and the corresponding electrostatic fields that are generated around it. Furthermore, as one can see in Figure 14(b), the measured escape distribution is much broader and higher in temperature than the initial birth distribution, which is significant for experimentalists who try to characterize the birth distribution by simply measuring those electrons that escape from the target.

Because the electrostatic fields surrounding the target have been shown to significantly affect the correspondence between the original electron birth distribution and the escaping distribution, one might expect that the target shape may also affect the distribution that experimentalists measure. A larger target will presumably result in a modified field structure as well as a different potential drop across the target, which will inevitably modify the ability of electrons to escape from the target. Because this effect will be significant to experimentalists due to the variety of target sizes they use for laser-target experiments that are conducted, we have investigated this issue by simulating several different targets of varying length.

We studied the effect of changes in disk radius from 100 μm, discussed above, to 200 μm and 500 μm. The latter was used to approximate an infinite conductor with a short at the boundary. The same isotropic hot electron distribution was used for all three cases, as discussed previously, consisting of hot electrons being promoted from the background over a 30fs Gaussian pulse with a total energy of 0.3J. The structure of the hot electron distribution involved use of the same isotropic Jüttner distribution with a 305 keV temperature.

Shown in Figure 15 is the hot electron density and electrostatic potential for each of the three target sizes at t = 800fs. What is immediately obvious from these plots is the increase in "escape shells" for larger and larger target sizes and the corresponding drop in potential. As similar effect was seen in simplified spherical model in section III. In brief, what happens is that for smaller target sizes, the hot electrons within the target reach the top edge and escape more quickly where the potential drop in this direction is lowest and creates a preferred path of least resistance. As a result, the target charges up and the potential plateaus not only more quickly but also at a higher level to reach a quasi-static equilibrium in which no remaining electrons within the target have sufficient energy to escape. On the other hand, larger targets require more time for the hot electrons within the target to escape from the top edge, which

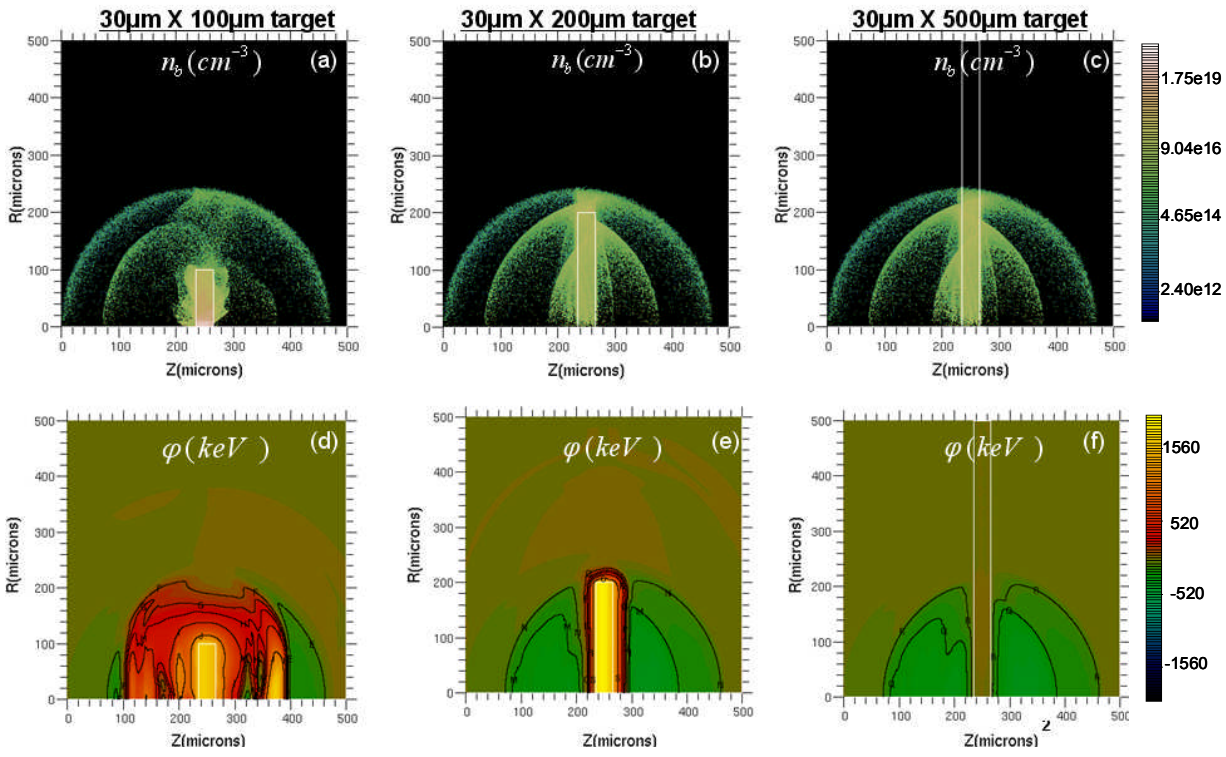

Figure 15. Hot electron density for three different target sizes (a-c) and the corresponding electrostatic potential (d-f) at 800fs.

Target Size	Escape Fraction
30μm x 100μm	4.5%
30μm x 200μm	12.0%
30μm x 500μm	42.5%

Table 2. Escape fractions for the three target sizes computed at the approximate time at which the electrostatic potential plateaus.

allows for a lower potential drop that enables more electrons to escape from the target before the potential plateaus and prevents further escape.

One can gain a little more insight into the effects of target size by computing the escape fraction and the energy spectrum of the escaping particles for the three target sizes. Shown in Table 2 are the escape fractions for the three target sizes at 700fs for the 30μm x 100 μm target, 900fs for the 30μm x 200 μm target, and 1ps for the target approximating an infinite conductor (30μm x 500 μm). At these times, the potential is approximately constant and the escape fraction has leveled off. As one can see, the escape fraction increases with target size, reaching a limiting value of approximately 43% for the infinite conductor case. This is in agreement with the observations discussed previously since smaller targets allow electrons to escape from the top edge more quickly, resulting in a larger potential drop across the target and preventing further electron escape early on. The energy spectrums of the hot electrons also reveal significant target size effects. Shown in Figures 16(a-c) are the energy spectra of the initial birth distribution in red with the escape distribution overlaid in black for each of the three target sizes. A log plot of these distributions has been included in Figures 16(d-f) for easier interpretation of these results. As one can see from the figure, the structures of the escape spectra for the 30μm x 100 μm and 30μm x 200 μm targets are very similar, consisting of much broader, higher temperature escape distributions compared to the initial birth distribution around the peak. Furthermore, the escape

distribution structure appears to be very similar to the initial birth distribution around the tail for both target sizes, suggesting that high-energy particles escaping the target are not significantly

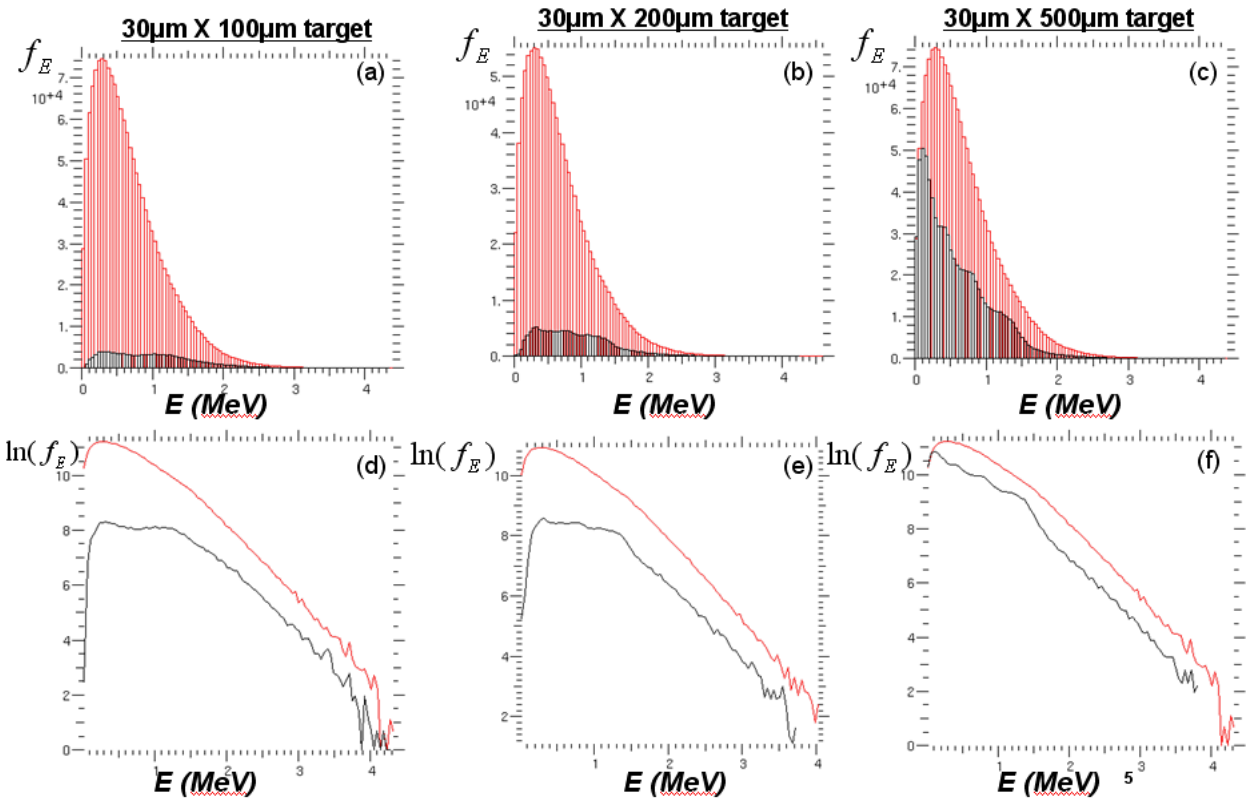

Figure16. Energy spectrum of the initial birth distribution (red) and the escape distribution (black) for each of the three target sizes (a-c) and the corresponding log plot of each (d-f).

altered by the fields surrounding the target. However, the energy spectrum of the escape distribution for the largest target (30µm x 500µm) appears to be relatively similar to the initial birth distribution. Based on the results in Figure15, one would expect this due the path of least resistance created by the short at the boundary and the absence of electron bursts escaping from the top edge in the previous cases. As a result, there are smaller fields and a lower potential drop across the larger target, resulting in less significant modifications of the initial birth distribution.

III. Effects of Angular Orientation of the Initial Electron Birth Distribution

Up to this point, the analysis has focused entirely on an isotropic hot electron birth distribution. However, in reality, the laser will be incident at some angle, which may influence the fraction of electrons leaving along the target surface, as quoted by Li et al. and other published works [4,5]. Because this laser angle of incidence naturally translates into a preferred drift direction of the hot electron birth distribution, we can implement this effect in LSP by simply adding a drift to the initially isotropic Jüttner distribution.

As mentioned previously, the original distribution consisted of a Jüttner distribution with a 305keV temperature (case A); however, we introduced two new distributions (cases B and C) to mimic the laser incidence angle that have an added drift in the Z- and R-directions, respectively. The disk has radius 100 microns and thickness 30 microns. The distribution associated with case B is initiated with a drift of 0.5c directed normal to the target to approximate normal laser incidence and the distribution associated with case C is initiated with a drift of 0.5c directed parallel to the target to approximate glancing laser incidence. Shown in Figure17 are phase space plots of the momentum distributions of the three cases.

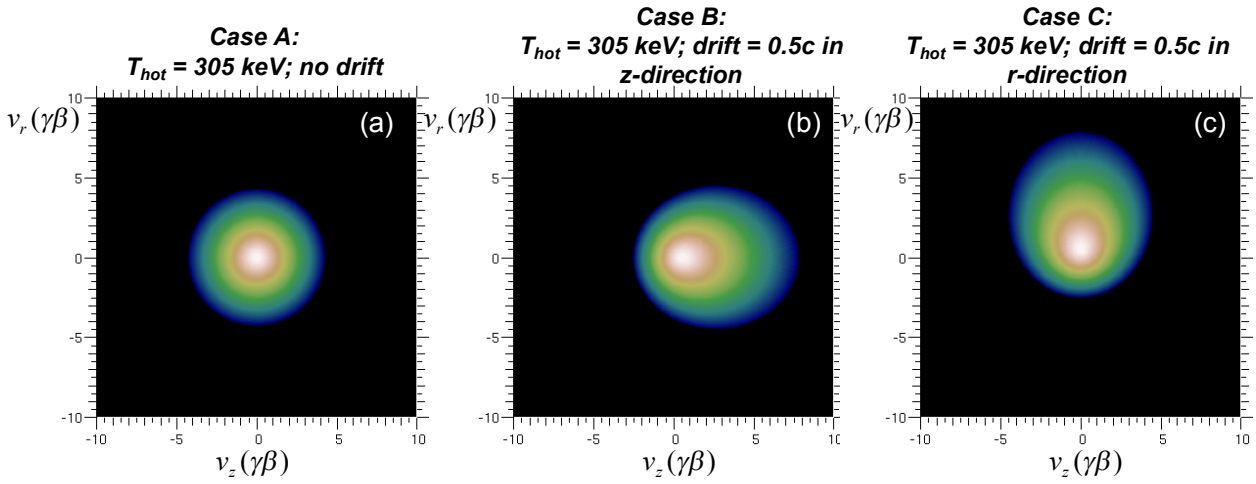

Figure 17. Momentum distributions of simulation cases A, B, and C with drifts of 0, 0.5c (z-direction), and 0.5c (r-direction), respectively.

The feature of greatest interest for comparison of the three cases is the escaping electron intensity as a function of angle with respect to the target center. Shown in Figure 18 is an equivalent series of histograms of the angular distribution of the escaping electron intensity, as

was done for the isotropic distribution, case A, in Figure 14. For the normally incident drift case, B, the structure is a little more broad and full compared to the isotropic case, as one would expect, while the parallel drift case C, has a structure which is slightly sharper, especially around the peak at θ =

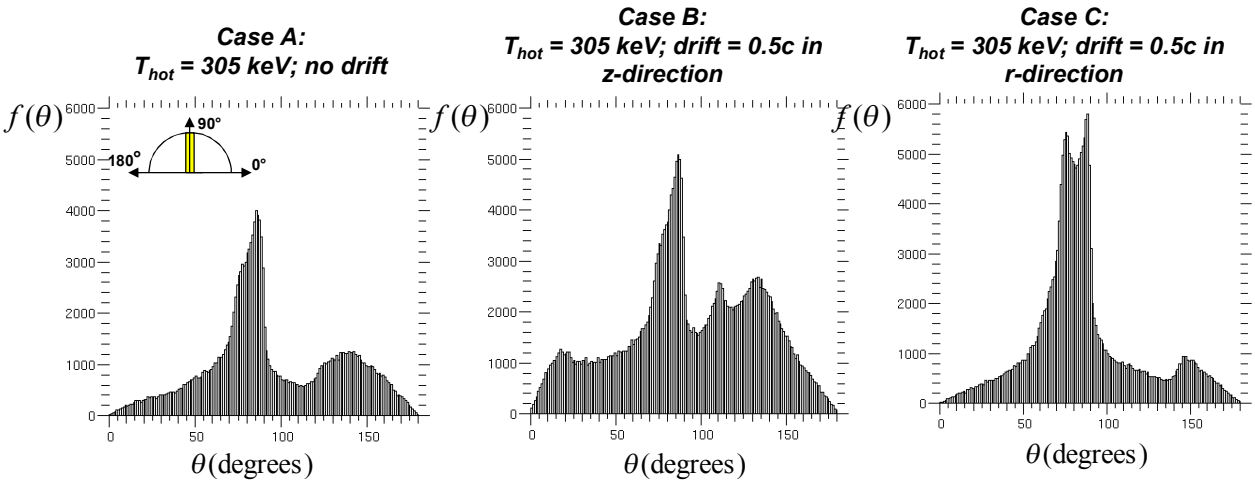

Figure18. Angular distribution of escaping electrons for cases A, B, and C at t = 500fs.

90º. Overall, though, the significant feature of interest is the clearly dominant peak at θ = 90º that exists for all three cases. A more quantitative analysis of this feature can be gained from Fig. 19 showing a comparison of the fraction of escape electrons being emitted within the surface escape angle, θ_{tsurf}, which has been defined by the coordinate system in the figure. As one can see from the table, the fractions of electrons escaping through this angle are comparable with differences being relatively minimal compared to those quoted by earlier publications [4,5]. What this suggests is that regardless of the initial angular orientation of the birth distribution, approximately the same fraction of electrons tend to escape along the top surface due to the lower potential drop.

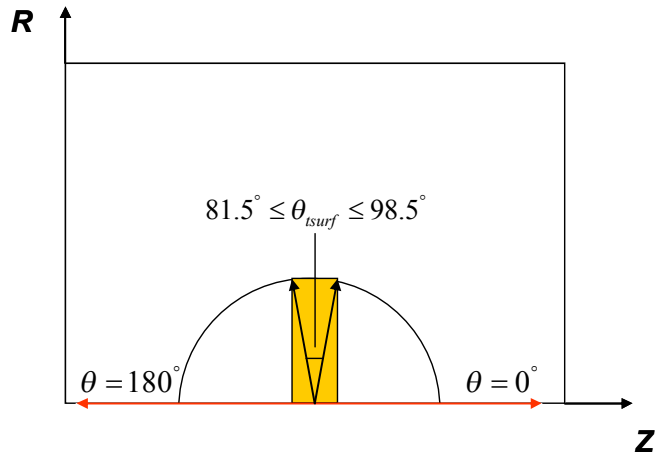

Case	Escape Fraction within θ_{tsurf}
A	40%
B	27.0%
C	50%

Fig. 19. Fractions of escaping electrons through θ_{tsurf} for simulation cases A, B, and C.

V. Conclusions

Our fully integrated explicit and hybrid implicit PIC simulations have shown that hot electron surface confinement is only a minor effect. In addition to finding no critical angle, we have also found that even for small angles of incidence, the fraction of electrons confined to the surface is quite small (~1%), suggesting that the cone target angle can be considered a minimal concern for design considerations. The discrepancy between these PIC results and the large surface fractions quoted from experimental measurements were clearly linked to the escaping electron phenomenon, which refers to significant differences in the measured (escaping) hot electron spectrum with respect to the original birth spectrum due to the generation of strong electrostatic self-fields. After re-computing the escape spectrum and the corresponding fraction that escaped from the target edge, our PIC results were found to be in approximate agreement with those quoted from experiment (50% vs. 50-60%%). Furthermore, this fraction was found to have only a minor dependence on the angular orientation of the initial birth spectrum and subsequent angle of laser incidence. In sum, our results have shown that the electrostatic field structure produced by the target is strongly dependent on target geometry. As a result, the escaping angular distribution that is measured by experimentalists will be significantly altered from the initial birth distribution and will largely depend on the shape of the targets being used.

Prepared by LLNL under Contract DE-AC52-07NA27344.

References

[1] M. Tabak, J. Hammer, M. Glinsky, W. L. Kruer, S. C. Wilks, J. Woodworth, E. M. Campbell, and M. D. Perry, Phys. Plasmas 1, 1626 (1994).

[2] P. Norreys, R. Allott, R. J. Clarke, J. Collier, D. Neely, S. J. Rose, M. Zepf, M.

Santala, A. R. Bell, K. Krushelnick, A. E. Dangor, N.C. Woolsey, R. G. Evans, H. Habara, T. Norimatsu, R. Kodama, Phys. Plasmas, 7, 3721 (2000).

[3] S.P. Hatchett, D. Clark, M. Tabak, R.E. Turner, C. Stoeckl, R.B. Stephens, H. Shiraga, K. Tanaka, "Hydrodynamics of conically guided fast ignition targets", *Fusion Science and Technology,* 49**,** 327 (2006).

[4] T. Nakamura et al., Phys. Rev. Lett., 93, 265002 (2004).

[5] Y. T. Li ,et.al., Phys. Rev. Lett., 96, 165003 (2006).

[6] E. Fill, Phys. of Plasmas, 12, 052704 (2005).

[7] D. R. Welch ,D.V.Rose,B.V.Oliver and R.E.Clark, Nucl. Inst. Meth., Phys. Res. A 464, 134 (2001).

[8] H. Ruhl, *Introduction to Computational Methods in Many Body Physics* (Rinton Press, Princeton, New Jersey, 2005).

[9] K.Yasuike,M.H.Key,S.P.Hatchett,R.A.Snavely,K.B.Wharton,Review of Scientific Instruments, **72**,1(2001)1236.

[10] B.Chrisman,Y.Sentoku and A.Kemp,Physics of Plasmas 15, 056309(2008).

[11] Y.Ping,et.al.,Phys.Rev.Lett. 100, 085004(2008).

[12] S.C.Wilks,W.L.Kruer,M.Tabak,A.B.Langdon,Physical Review Letters **69**,9(1992)1383.

[13] R.J.Mason and M.Tabak, Physical Review Letters **80**,3(1998)524

[14] Tatarakis,M.,et.al.,Nature **415**,6869(2002)280.

[15] Wagner,U.,et.al.,Physical Review E **70**,2(2004)26401-1-5.

[16] R.N.Sudan,Physical Review Letters **70**,20(1993)3075.

[17] B.F.Lasinski,A.B.Langdon,C.H.Still,M.Tabak and R.P.J.Town, Physics of Plasmas **16** (2009)012705.

[18] T.Nakamura,H.Sakagami,T.Johzaki,H.Nagatomo,K.Mima and J.Koga, Physics of Plasmas **14**(2007)103105.

[19] R.B.Campbell,J.S.Degroot,T.A.Mehlhorn, et.al., Physics of Plasmas **10**(2003)4169.

[20] Y.Sentoku,K.Mima,H.Ruhl,Y.Toyama,R.Kodama, and T.E.Cowan,Phys. Plasmas **11**,6(2004)3083.

[21] J.S.Green,et.al.,,Nature Physics 3,12(2007)823.

[22] T.Ma,Physics of Plasmas **16,**112702(2009).

[23] D.W.Forslund and J.U.Brackbill, Physical review Letters **48**(1982)1614.